**Ocean Science
Discussions**

High-resolution nested model for the Lebanese coastal area, Eastern Mediterranean: implementation and climatological runs

N. Kabbara[1], R. Sorgente[2], S. Natale[2], D. R. Hayes[3], and G. Zodiatis[3]

[1]National Center for Marine Sciences, P.O. Box 189 Jounieh, Lebanon
[2]International Marine Center, Loc. Sa Mardini Torregrande ORISTANO, CAP 09170, Italy
[3]Oceanography Centre, University of Cyprus, P.O. Box 20537, 1678 Nicosia, Cyprus

Correspondence to: D. R. Hayes (dhayes@ucy.ac.cy)

OSD

3, 373–396, 2006

**Nested model for
Lebanese coastal
area: climatological
runs**

N. Kabbara et al.

Title Page

Abstract | Introduction

Conclusions | References

Tables | Figures

◄◄ | ►►

◄ | ►

Back | Close

Full Screen / Esc

Printer-friendly Version

Interactive Discussion

EGU

Nested model for Lebanese coastal area: climatological runs

N. Kabbara et al.

Printer-friendly Version

Interactive Discussion

Abstract

As a part of the project Mediterranean Network to Assess and Upgrade Monitoring and Forecasting Activity in the Region (MAMA) we implemented a high resolution nested hydrodynamic model (1/40° horizontal grid, 16 sigma levels) for the coastal, shelf and open sea areas off the Lebanese coast, East Levantine Basin of the Eastern Mediterranean Sea. The Lebanese Shelf Model (LSM) is a version of the Princeton Ocean Model (POM). It is nested in a coarse resolution model the Aegean Levantine Eddy Resolving Model (1/20° horizontal grid, 25 sigma levels), ALERMO, that covers the Eastern Mediterranean. The nesting is one way so that velocity, temperature, and salinity along the open boundaries are interpolated from the relevant coarse model variables. Numerical simulations have been carried out under climatological surface and lateral forcing. Due to the relatively small domain, the results closely follow the simulation of the intermediate model with more details especially over the narrow shelf region. Simulations reproduce main circulation features and coastal circulation characteristics over the eastern Levantine shelf. This paper describes the modeling system setup, compares the simulations with the corresponding results of the coarse model ALERMO, and with the observed climatological circulation characteristics in the Levantine Basin off the Lebanese coast.

1 Introduction

The continental shelf at the eastern part of the Mediterranean Sea off Lebanon is relatively narrow (3–18 km) as compared to other Mediterranean regions because of the limited sediment drift in this area. The shelf is interrupted by a series of deep submarine canyons in its upper part which can be linked to a prominent fault pattern observed in the Lebanon Mountains (Emery and George, 1963; Geodicke, 1972). Direct current measurements conducted along the Lebanese coast reveal a predominantly bathymetry-following, north-northeastward flow and anticyclonic eddy features that fol-

low the coast (Kibar and Sokolov, 1988). Data obtained in the 1960s, 1970s and 1980s (Oren, 1970; Ovchinnikov et al., 1976, Hecht et al., 1988) indicated an anticyclonic circulation in the southern part of the Eastern Mediterranean. Hydrographic observations made by the Physical Oceanography of the Eastern Mediterranean (POEM)
5 cruises (Ozsoy et al., 1991, 1993; The POEM Group, 1992; Brenner, 1993) and the EDDY cruises (Brenner et al., 1991; Brenner, 1993) indicate that the circulation in the offshore waters (deeper than 1000 m) in the central latitudes of the Levantine Basin is predominantly anticyclonic due to the presence of a recurrent gyre system. In addition to the extensive data collection programs that have been conducted through the
10 Eastern Mediterranean over the past 15–20 years, various efforts have focused on modeling the circulation of the Mediterranean Sea and its sub-basins (e.g. Tziperman and Malanotte-Rizzoli, 1991; Roussenov et al., 1995; Zavatarelli and Mellor, 1995; Wu and Haines, 1998; Lascaratos and Nittis, 1998) but the essential step was done within the framework of the Mediterranean Forecasting System (MFS) promoted by The Eu-
15 ropean Global Ocean Observing System (EuroGOOS, 1997) for the implementation of operational oceanography in the Mediterranean Sea. The Mediterranean Forecasting System Pilot Project (Pinardi et al., 2003), MFSPP, represented the first phase in the realization of this goal and aimed for the development of an operational forecasting system for the Mediterranean Sea based upon three components: a near real time ob-
20 serving system, numerical forecasting systems at basin scale and for regional areas, and a forecast products dissemination/exploitation system. The MFSPP project has continued as the Mediterranean Forecasting System – Toward Environmental Prediction (MFSTEP). The modeling system of MFSTEP consists of: the full Mediterranean general circulation model (Pinardi et al., 2003), at approximately 7 km resolution, re-
25 gional models for different regions of the Mediterranean Sea such as the Aegean Levantine Eddy Resolving Model (Korres and Lascaratos, 2003), ALERMO, for the Eastern part of the Mediterranean Sea, at approximately 3 km resolution, and a collection of shelf/coastal models for different areas of the Mediterranean Sea. The hierarchy of models are linked using a one-way nesting technique.

Nested model for Lebanese coastal area: climatological runs

N. Kabbara et al.

Title Page

Abstract | Introduction

Conclusions | References

Tables | Figures

◄◄ | ►►

◄ | ►

Back | Close

Full Screen / Esc

Printer-friendly Version

Interactive Discussion

Within this activity and in cooperation with the International Marine Centre – Sardinia, we have developed a high resolution model for the shelf and open sea areas of Lebanon. The aim of this paper is to describe the modeling system setup; illustrate climatological simulations; compare the results with the corresponding results of the coarse model ALERMO and with the observed climatological circulation characteristics in the shelf and open sea area of Lebanon.

2 Model set-up

The model that has been used in this work is the Princeton Ocean Model (POM). POM has been extensively described in literature (e.g. Blumberg and Mellor, 1983, 1987; Oey et al., 1985a, b; Galperin and Mellor, 1990a, b; Mellor and Ezer, 1991a) and used to simulate the circulation in various regions of the world, including the Mediterranean Sea (e.g. Zavatarelli and Mellor, 1995; Lascaratos and Nittis, 1998). POM is a primitive equation, three-dimensional, time-dependent hydrodynamic model. It consists of prognostic equations for the two components of the horizontal momentum, potential temperature, salinity, and the free surface and three diagnostic equations consisting of the hydrostatic equation, an equation of state, and the vertical velocity, which is derived from the mass continuity equation. The model uses the Mellor-Yamada turbulence closure sub-model in order to provide the vertical turbulent mixing coefficients (Mellor and Yamada, 1982). The horizontal diffusion for momentum is described by Smagorinsky horizontal diffusion formula (Smagorinsky, 1993). The model comprises a bottom following sigma coordinates, and a split mode time step. The model horizontal grid uses curvilinear orthogonal coordinates and an "Arakawa C" differencing scheme.

2.1 Equations of the model

The equations of motion are Eqs. (1), (2) and (3); continuity is Eq. (4); conservation of temperature is Eq. (5); conservation of salinity is Eq. (6). Hydrostatic and Boussinesq

Nested model for Lebanese coastal area: climatological runs

N. Kabbara et al.

approximations are invoked. The equation of state, Eq. (7), is an adaptation of the UNESCO equation of state revised by Mellor (1991).

$$\frac{\partial u}{\partial t} + \left[u\frac{\partial u}{\partial x} + v\frac{\partial u}{\partial y} + w\frac{\partial u}{\partial z} \right] - fv = \frac{1}{\rho}\frac{\partial p}{\partial x} + \frac{\partial}{\partial z}\left(K_M \frac{\partial u}{\partial x} \right) + \frac{\partial}{\partial x}\left[2A_M \frac{\partial u}{\partial x} \right] + \frac{\partial}{\partial y}\left[A_M \left(\frac{\partial u}{\partial y} + \frac{\partial v}{\partial x} \right) \right] \quad (1)$$

$$\frac{\partial v}{\partial t} + \left[u\frac{\partial v}{\partial x} + v\frac{\partial v}{\partial y} + w\frac{\partial v}{\partial z} \right] + fu = \frac{1}{\rho}\frac{\partial p}{\partial y} + \frac{\partial}{\partial z}\left(K_M \frac{\partial v}{\partial z} \right) + \frac{\partial}{\partial y}\left[2A_M \frac{\partial u}{\partial y} \right] + \frac{\partial}{\partial x}\left[A_M \left(\frac{\partial u}{\partial y} + \frac{\partial v}{\partial x} \right) \right] \quad (2)$$

$$\rho g = -\frac{\partial p}{\partial z} \quad (3)$$

$$\frac{\partial u}{\partial x} + \frac{\partial v}{\partial y} + \frac{\partial w}{\partial z} = 0 \quad (4)$$

$$\frac{\partial \theta}{\partial t} + \left[u\frac{\partial \theta}{\partial x} + v\frac{\partial \theta}{\partial y} + w\frac{\partial \theta}{\partial z} \right] = \frac{\partial}{\partial z}\left(K_H \frac{\partial \theta}{\partial z} \right) + \frac{\partial}{\partial x}\left(A_H \frac{\partial \theta}{\partial x} \right) + \frac{\partial}{\partial y}\left(A_H \frac{\partial \theta}{\partial y} \right) \quad (5)$$

$$\frac{\partial S}{\partial t} + \left[u\frac{\partial S}{\partial x} + v\frac{\partial S}{\partial y} + w\frac{\partial S}{\partial z} \right] = \frac{\partial}{\partial z}\left(K_H \frac{\partial S}{\partial z} \right) + \frac{\partial}{\partial x}\left(A_H \frac{\partial S}{\partial x} \right) + \frac{\partial}{\partial y}\left(A_H \frac{\partial S}{\partial y} \right) \quad (6)$$

$$\rho = \rho(T, S, p) \quad (7)$$

The vertical mixing coefficients K_M, K_H are calculated using the Mellor and Yamada (1982) turbulence closure scheme. The horizontal diffusion coefficients A_M are calculated using the Smagorinsky formula (Smagorinsky, 1993),

$$A_M = C\Delta x \Delta y \sqrt{ \left(\frac{\partial u}{\partial x} \right)^2 + \frac{\left(\frac{\partial v}{\partial x} + \frac{\partial u}{\partial y} \right)^2}{2} + \left(\frac{\partial v}{\partial y} \right)^2 } \quad (8)$$

The model domain and bathymetry are shown in Fig. 1. It covers the region from 34.46–35.985° E and 32.96–34.735° N. The horizontal grid resolution is 1/40° in longitude and

Nested model for Lebanese coastal area: climatological runs

N. Kabbara et al.

EGU

latitude (62×72 grid points). In the vertical direction we used 16 layers. The sigma levels are more closely spaced in the topmost layer. For the bathymetry, the source is DBDB1 database (whole Mediterranean, 1/60°), adapted to our model through a bilinear horizontal interpolation. The minimum depth is 5 m. The coarse or intermediate model ALERMO covers the region 28–36° E and 30.7–37.0° N, and has a resolution of 1/20° in both latitude and longitude.

2.2 Lateral open boundary conditions

The Lebanese shelf model (LSM) has three open boundaries: north, south, and west. In order to find the boundary conditions for LSM at these three open boundaries, LSM was nested in ALERMO. The time-varying ALERMO data (u, v, $ubar$, $vbar$, T, S) were interpolated bilinearly to the open boundaries of LSM. In order to avoid inaccuracies in the interpolation which can generate errors leading to distortions of the model solution at the open boundaries or to violation of mass conservation (Pullen, 2000), an integral constraint was imposed on the interpolated normal velocity across the open boundaries so that the cross sectional area flux across the entire boundary is preserved. This constraint for the interpolated normal velocity takes the form

$$\int_{l_1}^{l_2}\int_{H_c}^{\eta_c} U_c\,dz\,dl = \int_{l_1}^{l_2}\int_{H_h}^{\eta_h} U_f^{\text{corr}}\,dz\,dl \tag{9}$$

where l is the horizontal coordinate along the open boundary with end points l_1 and l_2, the superscript corr refers to the adjusted or corrected interpolated normal velocity. Superscripts c and h refer to the coarse (ALERMO) and high (LSM) resolution models respectively.

The LSM was nested to ALERMO as follows:

1. Free surface elevation is not nested: zero-gradient condition.

2. For the normal barotropic velocities (depth averaged) the following equation was applied (Pinardi et al., 2003):

$$V_h = \frac{H + \eta_c}{H + \eta_h} V_c + \varepsilon \sqrt{\frac{g}{H}} (\eta_h - \eta_c) \tag{10}$$

Where $\varepsilon = 1$ for a northern boundary and $\varepsilon = -1$ for a western or southern boundary.

3. Tangential total and barotropic velocities were set to zero.

4. Total normal velocities are specified by the interpolation of the coarse resolution model field to the finer model grid

$$V_c = V_h \tag{11}$$

5. For inflow conditions, T and S at the boundary of the fine grid are specified by the coarse model solution:

$$T_c = T_h; S_c = S_h \tag{12}$$

whereas for outflow conditions, an upstream advection scheme has been used:

$$\frac{\partial(T,S)}{\partial t} + U \frac{\partial(T,S)}{\partial x} = 0 \tag{13}$$

2.3 Surface and bottom boundary conditions

Monthly means of wind stress, heat and water fluxes on the sea surface were calculated from the ECMWF 6-hourly Re-Analysis (ERA) data set covering the period 1979–1993.

EGU

See Korres and Lascaratos (2003) or Sorgente et al. (2003) where the same forcing is used. The surface boundary conditions are:

$$K_V \frac{\partial \boldsymbol{u}}{\partial z}\Big|_{z=\eta} = \frac{\tau}{\rho_0} \tag{14}$$

$$K_h \frac{\partial T}{\partial z}\Big|_{z=\eta} = \frac{Q_{\text{sol}} - Q_{\text{up}}}{\rho C_p} + \frac{C_1}{\rho C_p}(T^* - T_{z=\eta}) \tag{15}$$

$$K_h \frac{\partial S}{\partial z}\Big|_{z=\eta} = S(E - P) + C_2(S^* - S_{z=\eta}) \tag{16}$$

The wind stress is the monthly mean τ from the climatology; ρ_0 is the air density. Figure 2 presents the monthly average climatological wind stress from ECMWF interpolated in the LSM grid for February (a) and August (b), representative of winter and summer. In both cases, the winds are primarily westerly, and are weaker in the northern part of the domain in winter. The mean wind stress over the study area is nearly 0.010 N m^{-2} in February and 0.013 N m^{-2} in August. The climatological annual cycle of mean wind stress (Fig. 3a) peaks in June and reaches a low in November. The solar radiation is Q_{sol} (from ERA), and Q_{up} is the upward heat flux which includes sensible, latent, and longwave heat fluxes. Flux Q_{up} was calculated according to Bignami et al. (1995) using ALERMO and ECMWF fields. The monthly climatological heat fluxes comprise the perpetual year cycle in Fig. 3. The heat gain is highest in June, while the heat loss is highest in December (Fig. 3b).

Precipitation E and evaporation P fluxes were calculated using Legates and Wilmott (1990). The seasonal cycle of the freshwater budget (evaporation – precipitation) has low values during winter and spring and high values during summer and autumn. Evaporation and precipitation reach maximum values in winter (Fig. 3c).

The additional two terms $C_1(T^* - T_{z=\eta})$ and $C_2(S^* - S_{z=\eta})$ are used for further adjustment of ALERMO fluxes for the LSM modeling area. In this study we used the values: $C_1 = 5$ W m^{-2}°C and $C_2 = 0.7$ m day^{-1}. The monthly mean sea surface temperature T^*

Nested model for Lebanese coastal area: climatological runs

N. Kabbara et al.

Title Page

Abstract	Introduction
Conclusions	References
Tables	Figures

◄◄　　　►►

◄　　　►

Back　　　Close

Full Screen / Esc

Printer-friendly Version

Interactive Discussion

EGU

and salinity S^* were calculated from the Mediterranean climatological dataset Med6 (Brankart and Pinardi, 2001). These terms relax the temperature and salinity of the upper layer of the model ($z=\eta$) to the climatology. At the ocean bottom the boundary condition is based on a quadratic drag formulation.

All data (τ, T^*, S^*, Q_{sol}, Q_{up}, E, and P) have been interpolated into the high-resolution grid through bilinear horizontal interpolation. Smoothing with a 5-point Laplacian filter has been used. Also a linear time interpolation is needed, from the time step of these data to the time step of the model (4 s).

3 Results and discussion

The model started from 1 January with integrations running for three successive years, using the perpetual year surface and lateral boundary conditions as described in the previous section. The simulated circulation in the Lebanese shelf and open sea area presented in this work refers to the third year of the perpetual run of the model.

Figure 4 shows the evolution of the domain mean kinetic energy, temperature, and salinity during the three years of integration. The evolution of the three integral quantities shows that the model quickly reached an equilibrium state in the form of a repeating annual cycle. The kinetic energy annual cycle has minimum values in May, and a peak in July, gradually decreasing through December to the following May (Fig. 4a). The pattern follows that of mean wind stress, but with about one month of lag and more variability. The large role of surface kinetic energy in total kinetic energy is evident. The initial adjustment period during the first year allowed the mean kinetic energy to increase from low values. The domain mean temperature reflects the seasonal cycle of the upper layers and has a maximum in late July to early August and a minimum in late February to early March (Fig. 4b). There is a small relative maximum of temperature in early January of each year. This is probably an artifact due to a discontinuity in the repeating cycle of heat flux at the start of each perpetual year (Brenner, 2003). The domain mean salinity annual cycle has a maximum in late January when the relatively

saline Levantine Intermediate Water (LIW) dominates the upper 200 m (Fig. 4c). The low integrated salinity in late summer is associated with the inflow of Atlantic Water (AW). It should be noted that LIW is not formed locally. (Indeed, in the period of the high salinity double peak from December though May, precipitation dominates or bal-
5 ances evaporation in Fig. 3c.) The annual cycle of salinity seems to be more related to the lateral boundary conditions than the surface forcing.

Simulated temperature and salinity profiles are compared with ALERMO climatology at two points A and B (Fig. 1) in the model domain off Jounieh Bay. Point A is located at (34° N, 34.8° E) and point B is located at (34° N, 35.4° E). The modeled profiles are
10 taken from 10-day averaged fields for 10–20 of the month for February and October (Fig. 5). The modeled temperature and salinity profiles compare well with ALERMO, confirming the ability of the model to reproduce the seasonal cycle of temperature and salinity. At points A and B, temperature profiles are nearly coincident with the exception that in February, the thermocline is shallower in LSM, although of reasonable depth
15 for the winter period. Differences are generally less than 0.3°C. Salinity profiles are generally smoother in LSM, and the biggest differences usually occur just below the halocline, where ALERMO shows lower salinity than LSM. Differences are generally less than 0.04 ppt.

Simulated total velocity and scalar fields and the corresponding ALERMO results are
20 shown in Figs. 6–9. In panel (a) of each figure are the 10-day means of LSM, while the corresponding ALERMO fields interpolated to LSM grid are in panel (b). The over-all results of the high-resolution model and the intermediate model are similar in all cases although the high resolution model often presents more developed mesoscale structure. Along the shelf break, the near-surface current in general is directed along
25 the coast towards the north-northeast and attains appreciable 10-day average values of about 30–40 cm s^{-1}. The relatively small domain is tightly constrained by the in-termediate model's boundary conditions and the coast, yet some mesoscale structure appears in the interior of the fine resolution model. In particular, the instability of the coastal current evident in LSM generates an anticyclonic eddy which can be observed

in the middle of the domain (33.7° N, 34.8° E) during summer and autumn (Figs. 8 and 9). At that time, the eddy is seen to pinch off from the coastal current only in the LSM and completely within the LSM domain. It is not forced directly by ALERMO boundary conditions, such as the anticyclonic circulation visible at 33.5° N in Figs. 6–7. Coastal instabilities such as this have been observed from satellite in this region (see Fig. 4 of Zodiatis et al., 2005b).

Another anticyclonic eddy appears in the northern part of the domain during March and August (Figs. 7 and 8) with velocities as high as $35\,\text{cm s}^{-1}$. Again, this eddy is more fully developed in LSM and in both models appears to be the result of a pinched off meander in the coastal current. Investigations of the SE Levantine Basin within the CYBO-Cyprus Basin Oceanography cruises (Zodiatis et al., 2004, 2005a, b) reveal that an anticyclonic eddy was established between southeast of Cyprus and offshore Lebanon in March 2002. A similar structure has been observed from satellite in May 2002 (Zodiatis et al., 2005a). Climatological runs of the coastal area Cyprus (Zodiatis et al., 2003) also indicate the development of secondary anticyclonic eddies near the area of 34.5° N and 35° E, particularly in spring and summer. Later, in September, a cyclonic eddy is found in the northern part of the domain (Fig. 9). This is consistent with the climatological simulations of Zodiatis et al. (2003) for October where the secondary anti-cyclonic eddy is replaced by a large cyclonic eddy. In Ozsoy et al. (1991), it is shown that the POEM-V cruise of 1987 and another cruise in 1988 encountered a large cyclonic eddy almost directly east of Cyprus during summer and late summer.

4 Conclusion

In this work we presented the implementation of a high resolution nested model for the coastal/shelf area of Lebanon (the Lebanese shelf model, LSM). The results of climatological simulations were compared with the coarse model ALERMO. Reasonable seasonal cycles in mean temperature and salinity were reproduced, as well as seasonal evolution of upper-layer stratification. The main known climatological circulation

features in the shelf area of Lebanon are produced by LSM. The dominant flow features of the LSM domain are: northeastward-flowing coastal current, two anticyclonic eddies from pinched off meanders of the coastal current, and a large cyclonic eddy driven by the boundary conditions in the northern part of the domain in September.

References

Bignami, F., Marullo, S., Santoleri, R., and Schiano, M. E.: Longwave radiation budget in the Mediterranean Sea, J. Geophys. Res., 100, 2501–2514, 1995.

Blumberg, A. F. and Mellor, G. L.: Diagnostic and prognostic numerical circulation studies of the South Atlantic Bight, J. Geophys. Res., 88, 4579–4592, 1983.

Blumberg, A. F. and Mellor, G. L.: A description of a three-dimensional coastal ocean circulation model, in: Three-Dimensional Coastal Ocean Circulation Models, edited by: Heaps, N. S., Coastal Estuarine Sci., vol. 4, 1–16, AGU, Washington, D.C., 1987.

Brankart, J. M. and Pinardi, N.: Abrupt cooling of the Mediterranean Levantine Intermediate Water at the beginning of the 1980's: Observational evidence and model simulation, J. Phys. Oceanogr., 31, 2307–2320, 2001.

Brenner, S., Rozentraub, Z., Bishop, J., and Krom, M.: The mixed layer/thermocline cycle of a persistent warm core eddy in the Eastern Mediterranean, Dynamics of the Atmosphere and Oceans, 15, 455–476, 1991.

Brenner, S.: Long-term evolution and dynamic of a persistent warm core eddy in the Eastern Mediterranean Sea, Deep-Sea Research II, 40(6), 1193–1206, 1993.

Brenner, S.: High-resolution nested model simulations of the climatological circulation in the southeastern Mediterranean Sea, Ann. Geophys., 21, 267–280, 2003.

EuroGOOS: The strategy for EuroGOOS, EuroGOOS Pub., 1, 132, 1997.

Emery, K. O. and George, C. J.: The shores of Lebanon, Woods Hole Oceanogr. Inst., Contr., No. 1385, 1963.

Goedicke, T. R.: Submarine canyons on the Central Continental Shelf of Lebanon in The Mediterranean Sea, edited by: Stanley, D. J., Dowen, Hutchington Ross, Stroudsburg, Penn., 1972.

Galperin, B. and Mellor, G. L.: A time-dependent, three-dimensional model of the Delaware

Nested model for Lebanese coastal area: climatological runs

N. Kabbara et al.

Bay and River. Part 1: Description of the model and tidal analysis, Estuarine, Coastal and Shelf Sci., 32, 231–253, 1990a.

Galperin, B. and Mellor, G. L.: A time-dependent, three-dimensional model of the Delaware Bay and River. Part 2: Three-dimensional flow fields and residual circulation, Estuarine, Coastal and Shelf Sci., 31, 255–281, 1990b.

Hecht, A., Pinardi, N., and Robinson, A.: Currents, water masses, eddies and jets in the Mediterranean Levantine Basin, J. Phys. Oceanogr., 18, 1320–1353, 1988.

Kibar, N. and Sokolov, C.: Temporal and spatial variability of current speeds in the Mediterranean Sea near the Lebanese coasts, Oceanology, 28(4), 561–570, 1988.

Korres, G. and Lascaratos, A.: An eddy resolving model of the Aegean and Levantine basins for Mediterranean Forecasting system Pilot Project (MFSPP): implementation and climatological runs, Ann. Geophys., 21, 205–220, 2003.

Lascaratos, A. and Nittis, K.: A high resolution three-dimensional numerical study of intermediate water formation in the Levantine Sea, J. Geophys. Res., 103, 18 497–18 511, 1998.

Legates, D. R. and Wilmott, C. J.: Mean seasonal and spatial variability in a gauge corrected global precipitation, Int. J. Climatol., 10, 121–127, 1990.

Mellor, G. L. and Yamada, T.: Development of a turbulent closure submodel for geophysical fluid problems, Rev. Geophys. Space Phy., 20, 851–875, 1982.

Mellor, G. L.: An equation of the state for numerical models of oceans and estuaries, J. Atmos. Oceanic Tech., 8, 607–611, 1991.

Mellor, G. L. and Ezer, T.: A Gulf Stream model and altimetry assimilation scheme, J. Geophys. Res., 96, 8779–8795, 1991a.

Oey, L.-Y., Mellor, G. L., and Hires, R. I.: A three-dimensional simulation of the Hudson-Raritan estuary. Part I: Description of the model and model simulations, J. Phys. Oceanogr., 15, 1676–1692, 1985a.

Oey, L.-Y., Mellor, G. L., and Hires, R. I.: A three-dimensional simulation of the Hudson-Raritan estuary. Part II: Comparison with observation, J. Phys. Oceanogr., 15, 1693–1709, 1985b.

Oren, O. H.: Seasonal changes in the physical and chemical characteristics and the production in the low trophic level of the Mediterranean Waters off Israel, Sea Fisheries Research Station, Haifa, Israel, Special Publication, 238 pp., 1970.

Ovchinnikov, I. M., Plakhin, A., Moskalenko, L. V., Neglyad, K. V., Osadchiy, A. S., Fredoseyev, A. F., Krivoscheya, V. G., and Voytova, K. V.: Hydrology of the Mediterranean Sea, Gidrometeoizdat, Leningrad, 375pp, 1976.

Title Page

Abstract | Introduction

Conclusions | References

Tables | Figures

◄◄ | ►►

◄ | ►

Back | Close

Full Screen / Esc

Printer-friendly Version

Interactive Discussion

Özsoy, E., Hecht, A., Ünlüata, Ü., Brenner, S., Oğuz, T., Bishop, J., Latif, M. A., and Rozentraub, Z.: A review of the Levantine Basin Circulation and its variability during 1985–1988, Dynamics of the Atmosphere and Oceans, 15, 421–456, 1991.

Özsoy, E., Hecht, A., Ünlüata, Ü., Brenner, S., Sur, H. I., Bishop, J., Latif, M. A., Rozentraub, Z., and Oğuz, T.: A synthesis of the Levantine Basin circulation and hydrography, 1985–1990, Deep Sea Res. II, 40(6), 1075–1119, 1993.

Pinardi, N., Allen, J. I., Demirov, E., De Mey, P., Korres, G., Lascaratos, A., Le Traon, P. Y., Maillard, C., Manzella, G., and Tziavos, C.: The Mediterranean ocean Forecasting System: First phase of implementation (1998–2001), Ann. Geophys., 21, 3–20, 2003.

Pullen, J. D.: Modeling studies of the coastal circulation off northern California, PhD dissertation in Oceanography, Oregon State Univ., 145, 2000.

The POEM Group (Robinson, A. R., Malanotte-Rizzoli, P., Hecht, A., Michelato, A., Roether, W., Theocharis, A., Ünlüata, Ü., A., Pinardi, N., Artegiani, A., Bishop, J., Brenner, S., Christianidis, S., Gacic, M., Georgopoulos, D., Golnaraghi, M., Hausmann, M., Junghaus, H.-G., Lascaratos, A., Latif, M. A., Leslie, W. G., Oğuz, T., Özsoy, E., Papageorgiou, E., Paschini, E., Rosentroub, Z., Sansone, E., Scarazzato, P., Schlitzer, R., Spezie, G.-C., Zodiatis, G., Athanassiadu, L., Gerges, M., and Osman, M.): General circulation of the Eastern Mediterranea, Earth Sci. Rev., 32, 285–309, 1992.

Roussenov, V., Stanev, E., Artale, V., and Pinardi, N.: A seasonal model of the Mediterranean Sea general circulation, J. Geophys. Res., 100, 13 515–13 538, 1995.

Smagorinsky, J.: Some historical remarks on the use of nonlinear viscosities, in: Large eddy simulations of complex engineering and geophysical flows, edited by: Galperin, B. and Orszag, S., Cambridge Univ. Press, 1993.

Sorgente, R., Drago, A. F., and Ribotti, A.: Seasonal variability in the Central Mediterranean Sea circulation, Ann. Geophys., 21, 299–322, 2003.

Tziperman, E. and Malanotte-Rizzoli, P.: The Climatological Seasonal Circulation of the Mediterranean Sea, J. Marine Res., 49, 411–434, 1991.

Wu, P. and Haines, W.: The general circulation of the Mediterranean Sea from a 100-year simulation, J. Geophys. Res., 103, 1121–1135, 1998.

Zavatarelli, M. and Mellor, G. L.: A numerical study of the Mediterranean Sea circulation, J. Phys. Oceanogr., 25, 1384–1414, 1995.

Zodiatis, G., Lardner, R., Lascaratos, A., Giorgiou, G., Korres, G., and Syrimis, M.: High resolution nested model for the Cyprus, NE Levantine Basin, eastern Mediterranean Sea: imple-

Nested model for Lebanese coastal area: climatological runs

N. Kabbara et al.

| Title Page	
Abstract	Introduction
Conclusions	References
Tables	Figures
◄◄	►►
◄	►
Back	Close
Full Screen / Esc	
Printer-friendly Version	
Interactive Discussion	

mentation and climatological runs, Ann. Geophys., 21, 221–236, 2003.

Zodiatis, G., Drakopoulos, P., and Gertman, I.: Modified Atlantic water in the Levantine Basin, 37th CIESM Congress Proceedings, Barcelona, Spain, 2004.

Zodiatis, G., Drakopoulos, P. Gertman, I., Brenner, S., and Hayes, D.: The Atlantic Water Mesoscale Hydrodynamics in the Levantine Basin, 27th CIESM Workshop Monograph – Strategies for understanding mesoscale processes, 2005a.

Zodiatis, G., Drakopoulos, P., Brenner, S., and Groom, S.: Variability of the Cyprus warm core eddy during the CYCLOPS project, Deep Sea Res. II, 52, 2897–2910, 2005b.

5

Nested model for Lebanese coastal area: climatological runs

N. Kabbara et al.

Title Page

Abstract	Introduction
Conclusions	References
Tables	Figures

◄◄ ►►

◄ ►

Back Close

Full Screen / Esc

Printer-friendly Version

Interactive Discussion

EGU
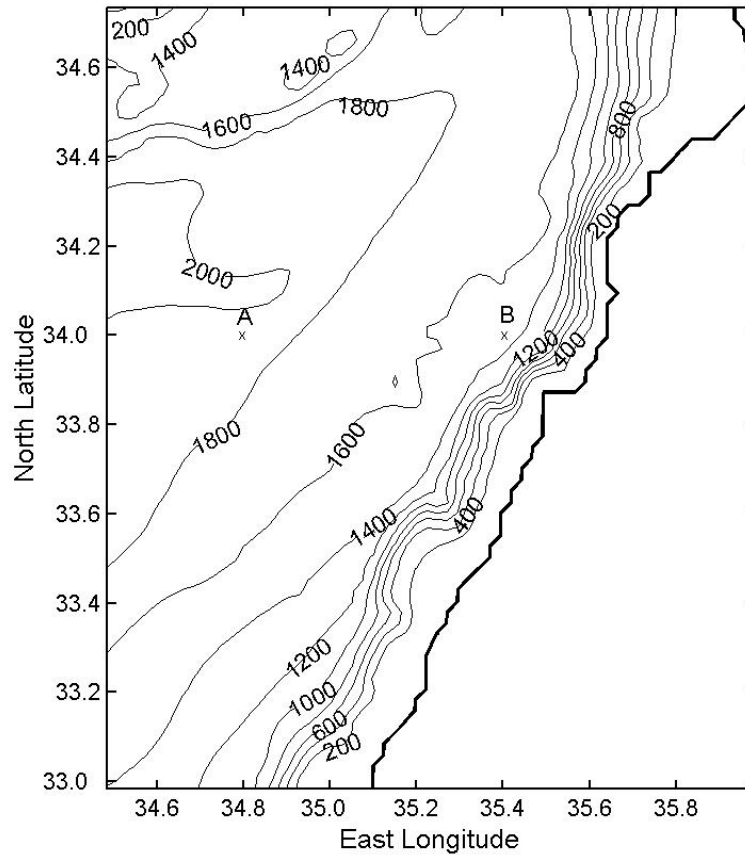
Fig. 1. Model domain and bathymetry of the study area. Model profiles will be plotted for point A (34° N, 34.8° E) and point B (34° N, 35.4° E).
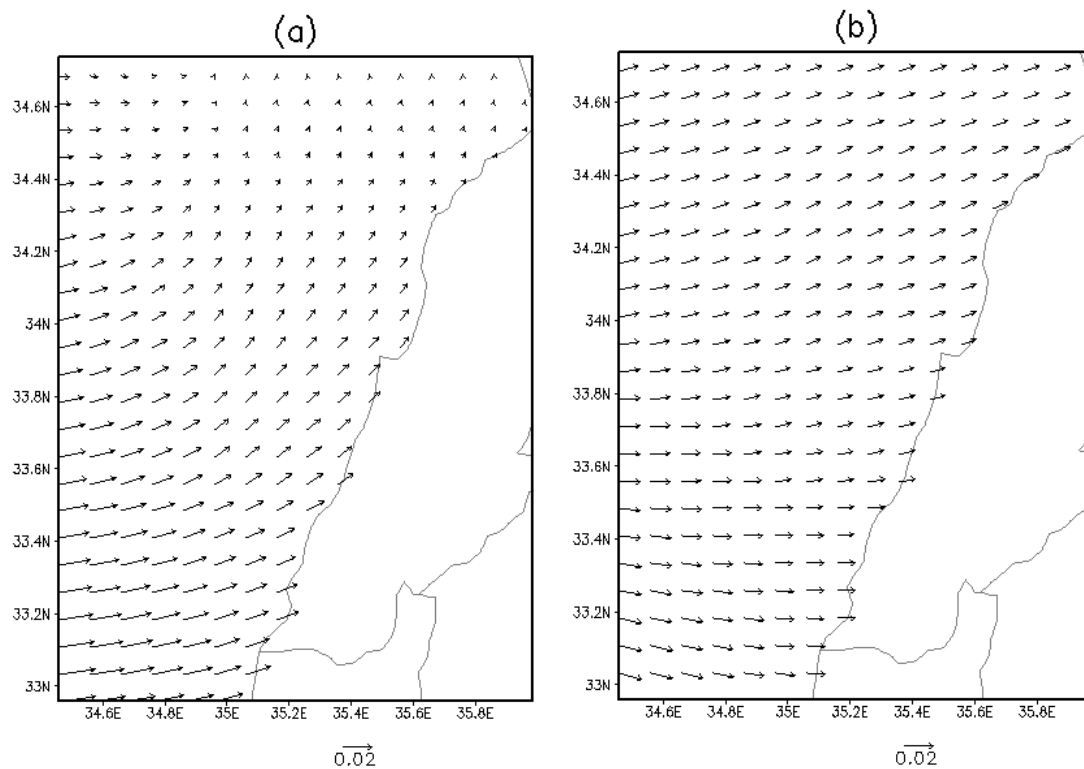
Fig. 2. Monthly average climatological wind stress. **(a)**: February, **(b)**: August. Units are N m^{-2}.
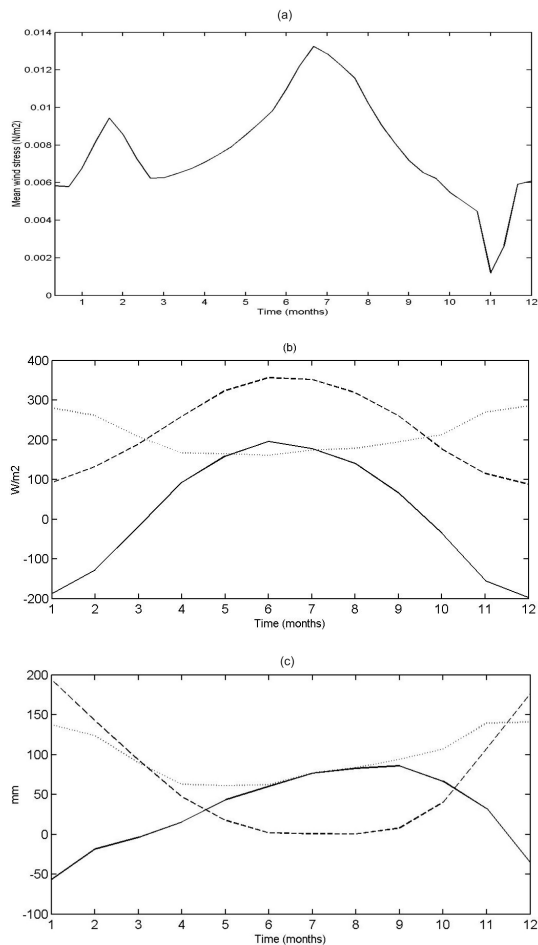
Fig. 3. Annual climatological cycle of **(a)**: the mean wind stress magnitude **(b)**: the total surface heat flux (solid line), solar radiation (dashed line), and the upward heat flux (dotted line), and **(c)**: the total fresh water flux (E-P) (solid line), precipitation (dashed line), and evaporation (dotted line).

390

Nested model for Lebanese coastal area: climatological runs

N. Kabbara et al.
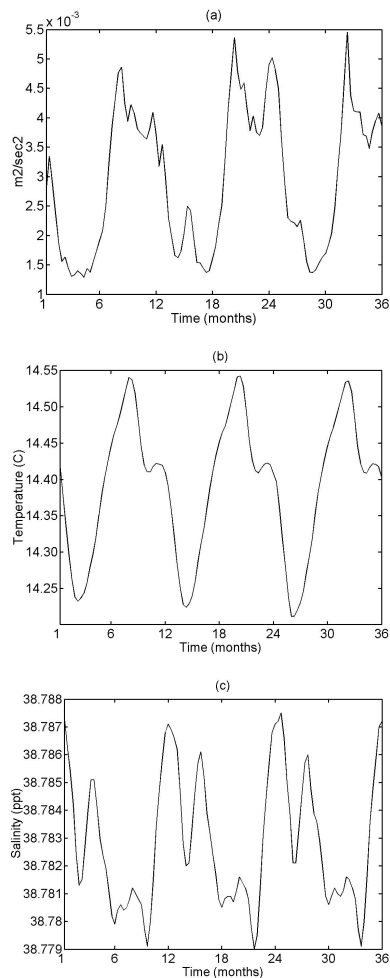
Fig. 4. Evolution of the domain means of **(a)** kinetic energy, **(b)** potential temperature, and **(c)** salinity during the three years of integration.

Title Page

Abstract   Introduction

Conclusions   References

Tables   Figures

◀   ▶

◀   ▶

Back   Close

Full Screen / Esc

Printer-friendly Version

Interactive Discussion

EGU
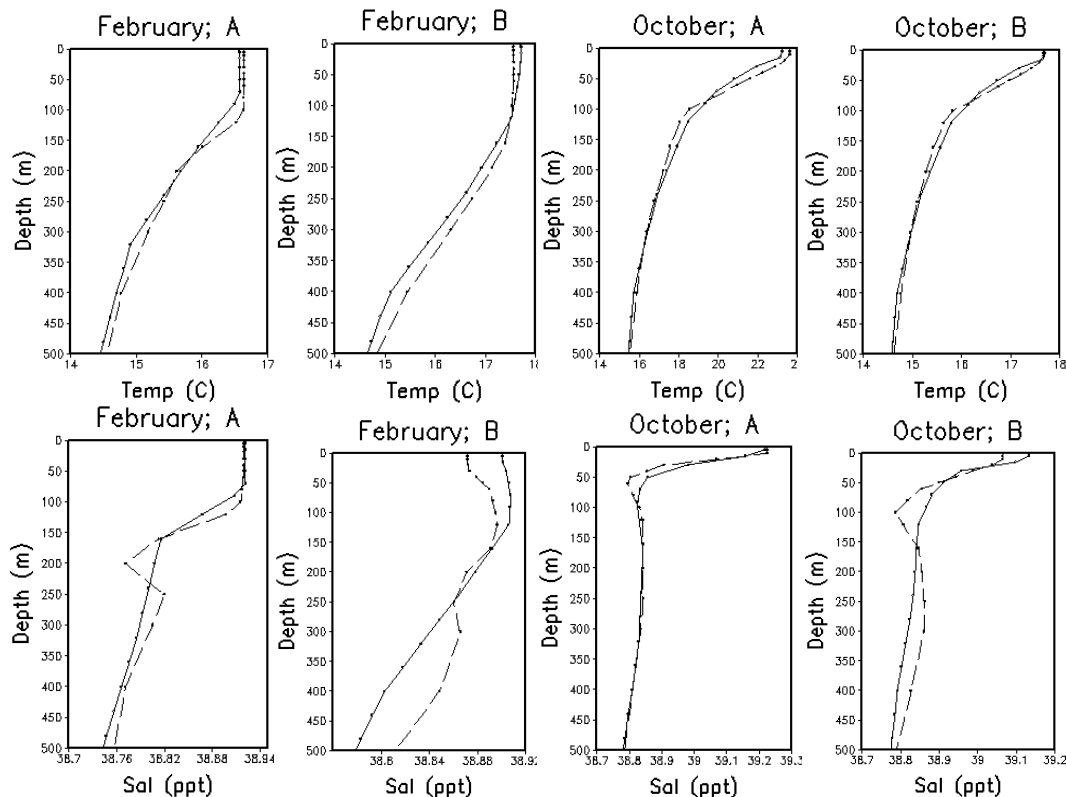
Fig. 5. Comparison between modeled (solid line) and ALERMO (dotted line) 10-day average temperature and salinity profiles at two locations of the modeled domain: B (34° N, 35.4° E) and A (34° N, 34.8° E), respectively, and at two different periods: 10–20 February and 10–20 October.

Title Page

Abstract　　Introduction

Conclusions　　References

Tables　　Figures

|◀　　　▶|

◀　　　▶

Back　　Close

Full Screen / Esc

Printer-friendly Version

Interactive Discussion
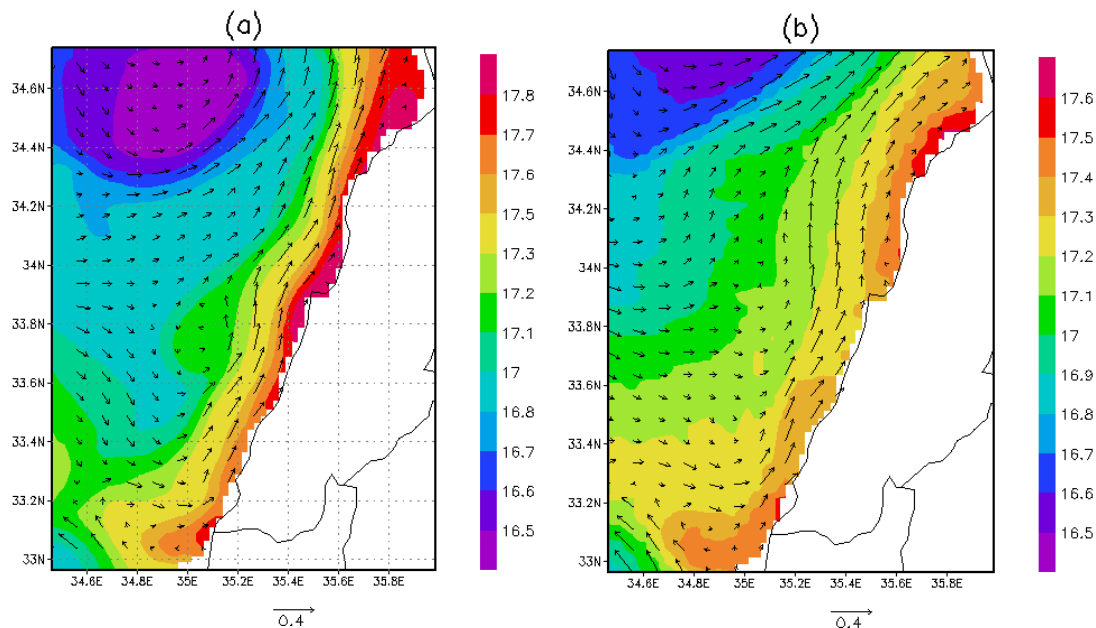
Fig. 6. Simulated potential temperature and velocity at 5 m: **(a)** 10-day average for 10–20 February, and **(b)** 10-day average for 10–20 February from the intermediate model.
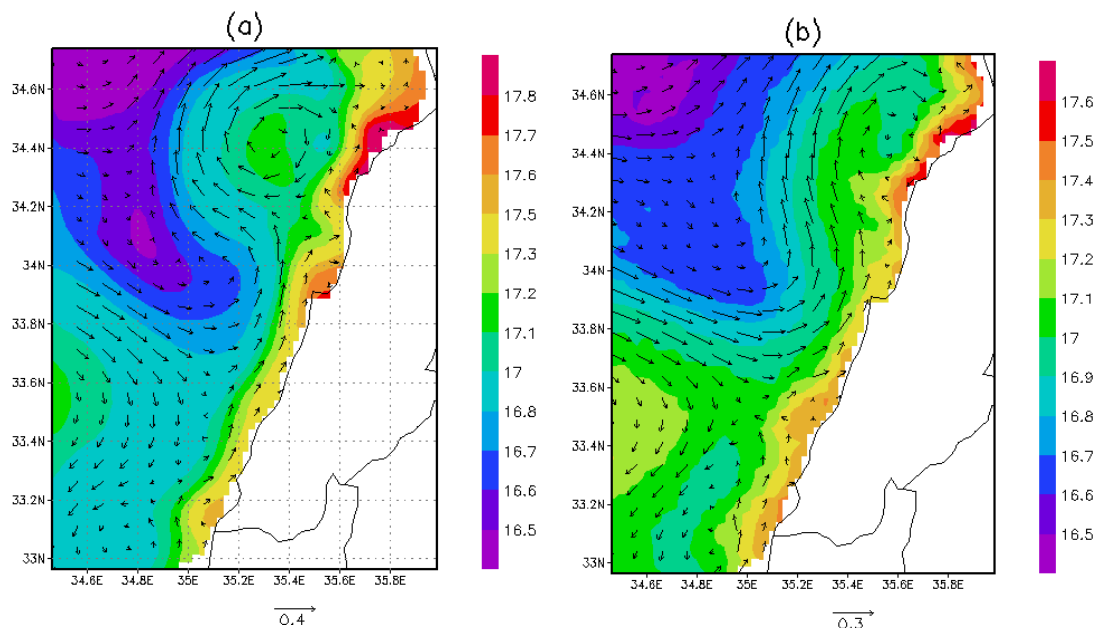
Fig. 7. Simulated potential temperature and velocity at 5 m: **(a)** 10-day average for 10–20 March, and **(b)** 10-day average for 10–20 March from the intermediate model.
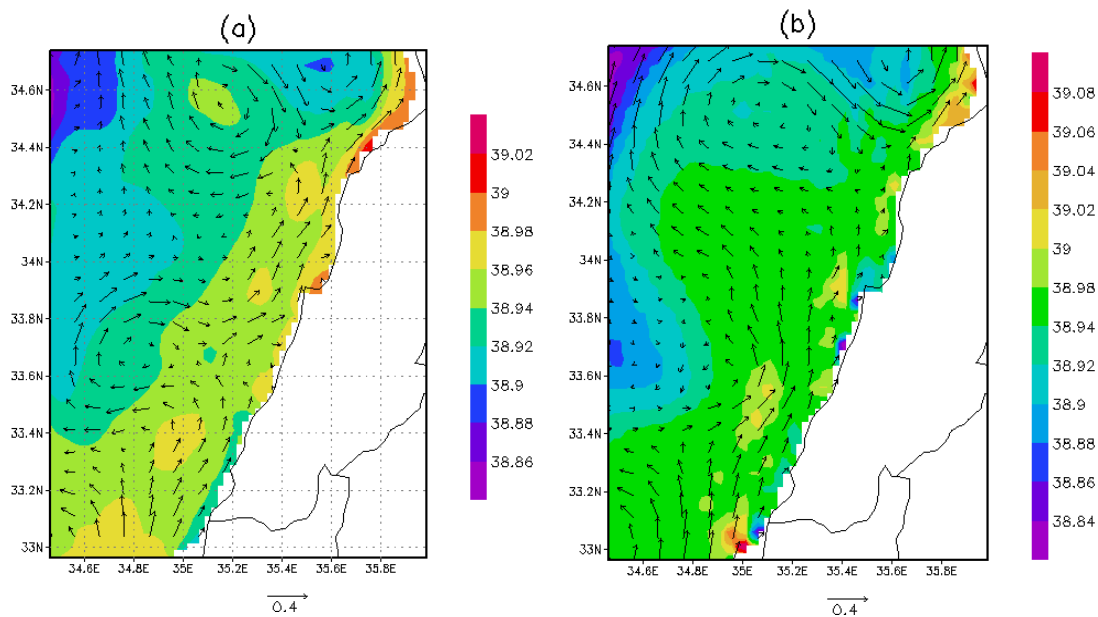
Fig. 8. Simulated salinity and velocity at 30 m: **(a)** 10-day average for 10–20 August, and **(b)** 10-day average for 10–20 August from the intermediate model.
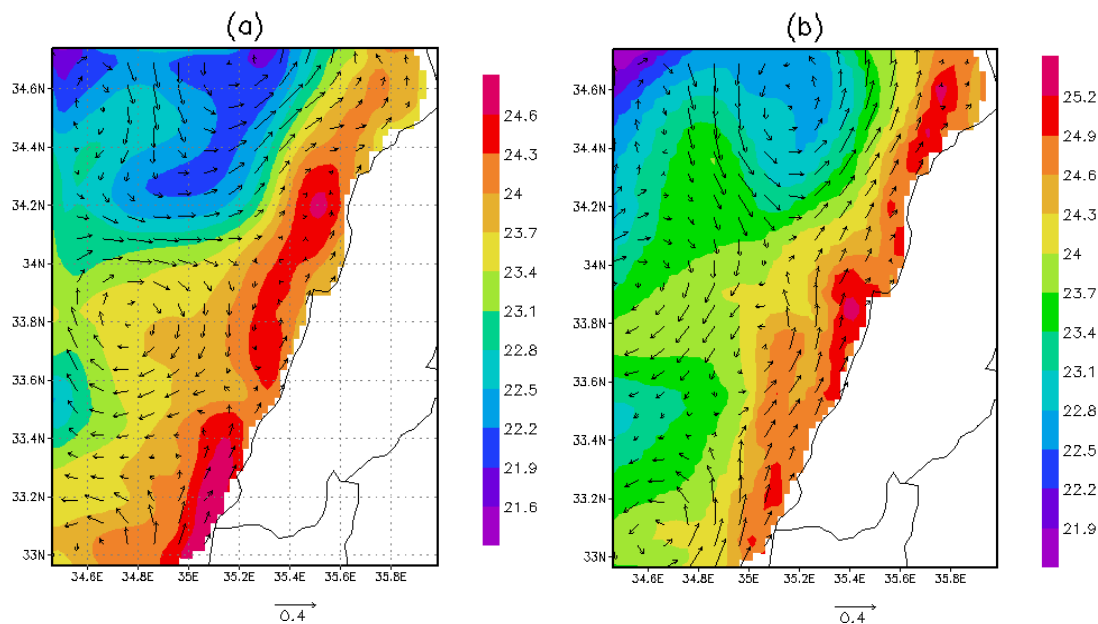
Fig. 9. Simulated potential temperature and velocity at 30 m: **(a)** 10-day average for 10–20 September, and **(b)** 10-day average for 10–20 September from the intermediate model.